Appl. Phys. A 78, 629–636 (2004)
DOI: 10.1007/s00339-003-2270-x

Applied Physics A
Materials Science & Processing

S. SCHLEMMER*
S. WELLERT
F. WINDISCH
M. GRIMM
S. BARTH
D. GERLICH✉

Interaction of electrons and molecules with a single trapped nanoparticle

Faculty of Natural Science, University of Technology, 09107 Chemnitz, Germany

Received: 18 October 2002/Accepted: 18 June 2003
Published online: 12 November 2003 • © Springer-Verlag 2003

ABSTRACT Highresolution nanoparticle mass spectrometry (NPMS) is used to study the interaction of electrons and molecules with the surface of a single, isolated particle stored in a three-dimensional quadrupole trap over weeks. IR-laser heating is employed as a fast temperature control. The kinetics of adsorption and desorption of molecules is studied for a 500-nm-diameter SiO_2 particle. A C_{60} multilayer film has been prepared during online NPMS monitoring. Emission probabilities for secondary electrons are determined for a bare particle and a particle with a 40-nm-thick layer of C_{60}. From the molecular desorption rates ($\sim$ fg/h) at constant temperature binding energies of multilayer 1.47-eV and submonolayer 1.53-eV C_{60} have been determined. Future perspectives of this new surface-science technique are discussed.

PACS 68.43.Mn; 81.15.Ef; 81.70.Pg; 81.70.Fy

1 Introduction

Solid-state surfaces are the interface between gas-phase atoms or molecules and those in solid state. Due to the high number density of reactants at the surface, interaction processes are much faster at this interface than in pure gas phase. Technically it is therefore often beneficial to increase the surface to volume ratio by using bulk samples of small particles in order to speed up chemical processes. Surfaces of small particles also play a pivotal role in many fields of science. Aerosols are important for the physics and chemistry of planetary atmospheres, one example being the ozone depletion in polar stratospheric clouds [1], another fine aerosols which pose potential health hazards [2]. The gas–grain interaction in the interstellar and circumstellar environment influences the time constant for particle agglomeration. This seemingly minor process is critical for the time to form agglomerates of particles, planetesimals and finally stars and planets [3]. Dust is also an active component in interstellar chemistry, e.g. molecular hydrogen is thought to be dominantly formed on small grains [4].

✉ Fax: +49-0371/531-3103, E-mail: gerlich@physik.tu-chemnitz.de
*Current address: P.O. Box 9513, 2300 RA Leiden, The Netherlands

Besides the large surface to volume ratio other finite size effects give small particles unique physical–chemical properties. These effects include for example their small heat capacity, the small radius of curvature of the surface and the influence of the charge state on the interaction with gas. Depending on the environment, e.g. interstellar space, such effects can lead to vastly different rates for physical–chemical processes, thus leading to unexpected pathways for chemical networks. For very small particles, < 10 nm, quantum size effects can govern their properties. In contrast to their importance only limited experimental work exists on isolated nanoparticles. Most of the work is dealing with large samples of particles. In aerosol science, condensation studies on fine particles in cloud chambers are one example [5].

Data from such experiments are dealing with averages over different particles with respect to size, shape or other characteristics. Therefore, experiments on isolated and single nanoparticles can reveal more fundamental results for understanding physical–chemical processes as opposed to bulk material or objects interacting with substrates.

In terms of surface-science techniques results obtained for large surfaces ($\sim$ cm^2) are often used to simulate the physics and chemistry of small particles' surfaces [6]. Due to the small quantities of material involved standard surface-science techniques can not be applied to single particles. As an example, temperature-programmed desorption (TPD) is the standard technique in surface science used to determine binding energies of adsorbates [7–9]. The desorbing molecules are usually detected by mass-spectrometric techniques. The detection sensitivity is therefore limited by the amount of desorbed material. This makes conventional TPD experiments from a single particle unfeasible. The experiment described here uses non-destructive and high-resolution mass spectrometry of a single, isolated 500-nm-diameter SiO_2 particle in order to overcome this and other limitations.

One benefit of nanoparticle mass spectrometry (NPMS) is the very small pressure increase due to the desorption of molecules in TPD-like experiments. In the present case one monolayer (ML) corresponds to about 10^6 molecules. Releasing one ML into the vacuum chamber at once leads to a temporary pressure increase of less than 10^{-14} mbar. Therefore the influence of gasphase species originating from the particle can be neglected.

The heat capacity of the particle is very small ($\sim 10^{-13}$ J/K). Selective heating of the particle is achieved by using an IR laser directed to the particle. Therefore, only small amounts of energy are necessary to heat the particle and the time scale for heating can be chosen very short. This allows very high temperature excursions, which are difficult to obtain otherwise. In addition, the heat load by the hot particle neither limits the temperature of the particle nor leads to an outgassing of the whole apparatus.

It has been demonstrated by Wuerker et al. more than forty years ago [10] that quadrupole confinement can be used to store single charged micron-sized particles over long times. Due to the electrodynamical trapping the particles are isolated from any interaction with a substrate; moreover, the threedimensional quadrupolar field leads to a very good localization of the particle in all directions, which makes it suitable especially for optical detection experiments. Starting in the 1970s this basic technique has been further developed to levitate particles, i.e. compensation of the gravitational force by a superimposed DC field. By this means the particles' charge-to-mass ratio, Q/M, can be determined with an accuracy in the percent range [11, 12]. The device is known as the electrodynamical balance (EDB). Today this instrument is combined with various other techniques, such as elastic and inelastic Mie scattering, in particular to study the physics and chemistry of tens of micron sized aerosols [13]. A recent review of EDB can be found in [14].

In contrast to the EDB technique a very recent development uses the quadrupolar trapping field in order to determine the nanoparticle's mass [15]. In the adiabatic limit the micromotion is much faster than the macromotion of the stored particle and the force field is derived from a harmonic potential with an eigenfrequency $\omega \propto Q/M$. Q/M is determined from a high-resolution frequency determination via optical detection of the modulation of scattered light from the laser-illuminated particle. The basic characteristics such as resolution, accuracy, long-time stability and linearity of the NPMS method are described in detail in [15]. Charge determination via secondary-electron emission is used to determine the absolute charge and mass of the trapped particle.

In the present setup the NPMS instrument has been extended by an effusive molecular beam source and IR-laser heating in order to facilitate a first controlled surface-science experiment of a single particle with a surface on the nanometer scale. In Sect. 2 NPMS online monitoring is described for a particle which has been further characterized by use of IR-laser heating. Details of the calculation of the particle's temperature are given. Secondary-electron emission is used to determine the particle's absolute charge and mass. The probability of secondary-electron emission is determined in Sect. 3. Preparation of a C_{60} multilayer adsorbate on a particle stored, characterized, prepared and manipulated for more than two weeks is given. IR-laser heating is then used to determine the binding energy of C_{60} in the multilayer and submonolayer regimes. In the discussion particular features of the combination of NPMS and TPD are evaluated and in Sect. 4 the applicability of other standard surface-science techniques to nanometer-scaled surfaces is discussed.

2 Experimental

A detailed description of the method of nanoparticle mass spectrometry has been given elsewhere [15]. Here we give only a brief summary of the main features of NPMS and describe some specific experimental details. For the present experiments IR-laser heating has been added to the setup in order to allow a controlled thermal treatment of the trapped particle. This situation is depicted in Fig. 1, which shows a schematic top view of the experimental setup. The housing of the three-dimensional quadrupole trap inside the vacuum chamber is shown in a horizontal cross-sectional view. The top and bottom cone-shaped electrodes are not seen. The eight small circles which surround the center of the trap are the eight vertical rod electrodes which approximate the function of the ring electrode typical for conventional Paul-trap designs. This geometry has been chosen in order to obtain a very open electrode design which allows the intersection of the trap with various tools. In Fig. 1 light from a diode laser and from a cw CO_2 laser is directed to the center of the trap passing between the rod electrodes. Also, the collection of the scattered visible light happens via these openings as shown in Fig. 1, detected by an avalanche photodiode and recorded with a real-time A/D converter. Additional tools such as the particle injector, an electron gun and an effusive source for the deposition of C_{60} molecules are not shown in Fig. 1 for clarity but they all point towards the center of the trap.

The CO_2 laser is a commercial 25-W laser emitting at 10.6 μm [16]. This wavelength is suitable to excite Si–O stretching vibrations in the SiO_2 particle thus substantially heating the stored particle. The actual power of the laser has been varied by tuning the duty cycle of its discharge. Practically it can be varied between 0.5 and 25 W. ZnSe windows and lenses have been used to focus the IR-laser beam to the center of the trap. There a maximum intensity of about 10^5 W/cm^2 can be achieved. Much more moderate intensities in the W/cm^2 range are sufficient to heat the particle to temperatures between 300 K and 500 K to desorb certain molecules from the surface. Typical beam diameter of 2 mm

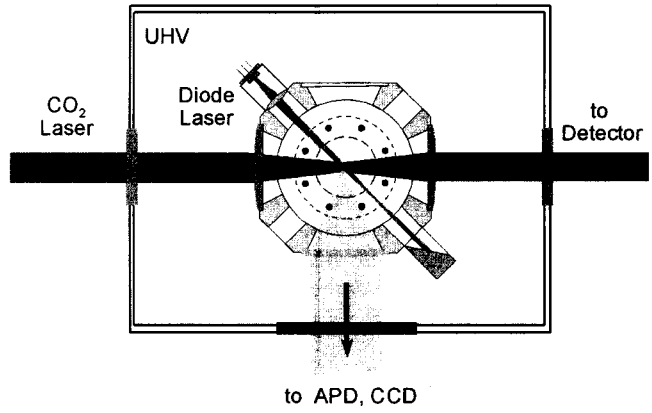

FIGURE 1 Top view schematic of the experimental setup. The particle is stored in the center of the trap, which is inside a UHV vacuum chamber and illuminated by the visible light from a diode laser. Scattered light is collected and detected (APD detector) in 45 degree sideways direction and used for the determination of the particle's Q/M ratio. IR light from a cw CO_2 laser is used to heat the particle in order to evaporate molecules from its surface

at the center of the trap guarantee a full illumination of the particle's trajectory. The temperature of the heated particle (sphere with radius a) has been calculated by balancing the absorbed power, $P_{abs}(\lambda_{Laser}) + P_{abs}(T_0)$, to the radiation emission power, $P_{em}(T)$:

$$P_{abs}(\lambda_{Laser}) + P_{abs}(T_0) = P_{em}(T)\,. \tag{1}$$

The absorbed power consists of the thermal radiation power of the surrounding walls at temperature T_0, with $P_{abs}(T_0) = P_{em}(T_0)$, and the absorbed power by the IR-laser light at $\lambda_{Laser} = 10.6\,\mu m$, which is given by

$$P_{abs}(\lambda_{Laser}) = Q_{abs} I_{Laser} \pi a^2\,. \tag{2}$$

Q_{abs} is the absorption efficiency for particles smaller than the wavelength λ (Rayleigh limit) [17]:

$$Q_{abs} = \frac{8\pi a}{\lambda} \mathrm{Im}\left[\frac{m^2-1}{m^2+2}\right]. \tag{3}$$

Typical absorbed powers from the IR laser are 100 pW for a 500-nm-diameter SiO_2 sphere ($\lambda = 10.6\,\mu m$, refractive index $m = n - i\,k, k = 0.10, n = 2.22$ [18]) at a laser intensity of $3\,W/cm^2$ [19].

The radiation emission power, $P_{em}(T)$, is given by

$$P_{em}(T) = 4\pi a^2 \int_0^\infty d\lambda\, \varepsilon(\lambda, a) P_\lambda(T)\,, \tag{4}$$

where $P_\lambda(T)$ is Planck's black-body distribution function for the energy flux:

$$P_\lambda(T) = \frac{2\pi hc^2}{\lambda^5\left[\exp\left(\frac{hc}{\lambda kT}\right) - 1\right]}. \tag{5}$$

The spectral emissivity, $\varepsilon(\lambda, a)$, of the particle is identical to the absorption efficiency Q_{abs}. Cooling by gas collisions accounts for only about 0.01 pW at 10^{-4} mbar of helium for a particle temperature of 500 K and has therefore been disregarded due to the high-vacuum conditions during the experiments.

Thus (1) establishes a relation between the laser intensity I_{Laser} and the temperature of the particle, T. In Table 1 the laser intensity is calculated which is necessary to heat the particle to a given temperature T. For SiO_2, emission in the near IR, visible and UV ranges can be neglected for T near room temperature. For the calculations of Table 1 the refractive index m in the relevant wavelength range 7–40 μm [18] has been accounted for. The temperature dependence of m has been neglected due to the comparably low particle temperatures during the measurements shown below. However, from the moderate intensities necessary to heat the particle to 500 K it is clear that particle temperatures in excess of 1000 K can easily be reached with the current IR laser.

The particle injector is a membrane that also serves as a reservoir for the commercially available SiO_2 particles [20]. Due to adhesive forces between the small particles isolation of an individual particle or small aggregate is happening by chance in the course of injection. In an improved source particles are suspended and isolated in a liquid and injected into the trap as individual micron-sized droplets. Droplet injection is well established in the field of aerosol science [13]. The number of particles per droplet will be controlled by the concentration of the suspension.

Upon storage the particle is illuminated by the diode laser. Due to the particle's motion inside the trap the scattered light is modulated at its eigenfrequencies, ω_r in the r direction and ω_z in the z direction, as has been described in [15]. These frequencies are determined by the fast Fourier transform (FFT) of the scattered light signal and used to determine the particle's charge to mass ratio, Q/M,

$$Q/M = \sqrt{2}\omega_r \Omega z_0^2 / V_0\,. \tag{6}$$

Here Ω is the driving frequency of the AC potential, $2V_0$ its amplitude, applied to the cone electrodes only, and z_0 is the quadrupole parameter. In the case of an ideal three-dimensional Paul trap $2z_0$ is identical with the distance between the end-cap electrodes. For the present boundary conditions of the trap $z_0 = 5.5$ mm has been determined using the ion-optics program SIMION [21].

T/K	I/W cm^{-2}
300	0.01
350	1.07
400	2.61
450	4.60
500	7.02

TABLE 1 Calculation of the necessary IR-laser intensity, I, necessary to heat the particle to the temperature, T. The temperature of the surrounding walls, T_0, is 295 K

3 Results and discussion

3.1 *Interaction of electrons with the particle*

As an example the online frequency measurement of a positively charged, single 500-nm-diameter SiO_2 particle is shown in Fig. 2. In this measurement the particle's charge state, Q, has been changed by electron bombardment. In the course of the six hours shown, the frequency is either constant or changes in a step-like fashion, indicating that the charging current is so low that charging due to secondary-electron emission happens in events with $\Delta Q = (N_2 - N_1)\,e$, where N_1 and N_2 are the number of elementary charges, e, carried before and after the charging process. Two events with $N_2 = N_1 - 1$ can be identified. Here the primary electron is stuck in the particle and no secondary electron is leaving. Due to the finite escape depth of secondary electrons the probability for these events is characteristic for the surface material of the particle, as will be shown below. From these electron-sticking events and the corresponding frequency change Δf_r the absolute number of charges on the particle has been determined using (6), $N = Q/e = -f_r/\Delta f_r$. Thus knowing the absolute charge state Q and the Q/M ratio according to (6), the absolute mass, M, of the particle has been determined. The particle characterized in Fig. 2 has a mass of 128.50 fg. At a given mass density of $2.0\,g/cm^3$ [20] this corresponds to a diameter of 497 nm, which is in good agreement with the

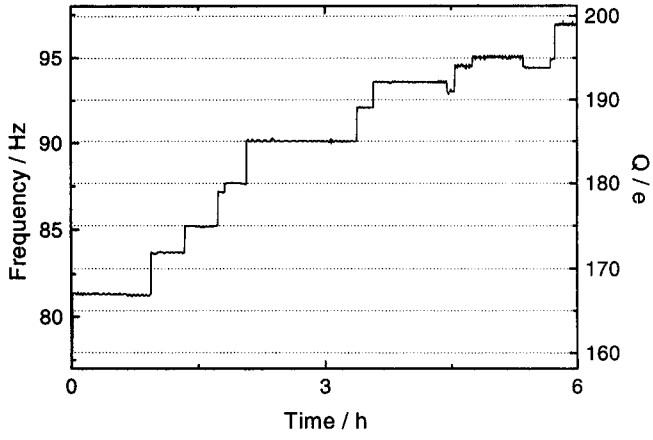

FIGURE 2 Mass determination of a single 500-nm-diameter SiO_2 particle. The eigenfrequency of the particle's motion in the r direction of the trap measured as a function of time is proportional to the Q/M ratio. The charge, Q, is changed during this six-hour measurement by electron bombardment due to secondary-electron emission in steps of multiple elementary charges, $\Delta Q = ne$. Q is inferred from the smallest step size $\Delta Q = -e$. This particle's mass is 128.50 ± 0.02 fg. The corresponding diameter of the particle is 497 nm

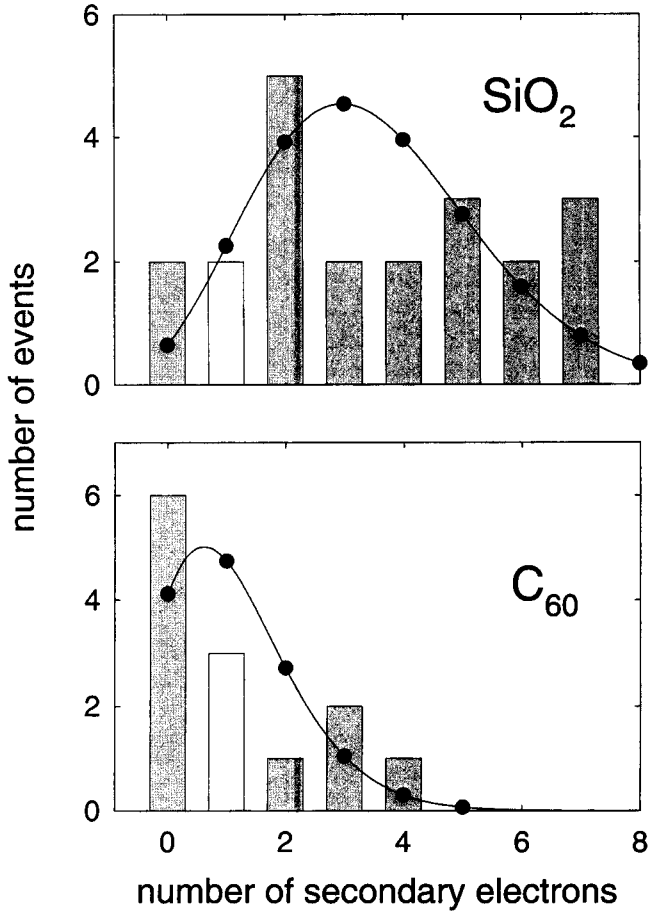

FIGURE 3 Distribution of the number of events of secondary-electron emission, $N(n)$, for a bare SiO_2 particle ($E_e = 590$ eV, $\delta = 3.48$) and for a SiO_2 particle covered with a 40-nm-thick layer of C_{60} ($E_e = 500$ eV, $\delta = 1.15$). The *numbers in brackets* are the electron energy, E_e, and the total yield, δ. *Solid lines* are least-square fits of a Poisson distribution to the histogram data

nominal diameter given by the manufacturer [20]. This particle has been further characterized by the use of laser heating. Results will be presented in Sect. 3.2.

Choosing the energy of the primary electrons, probabilities for emission of n secondary electrons, $P(n)$ has been determined. The number of events for the emission of secondary electrons, $N(n)$, of a bare SiO_2 particle ($E_e = 540$ eV) and one covered with a 40-nm layer of C_{60} ($E_e = 500$ eV) are shown in the histograms of Fig. 3. Details of how such a coverage is prepared and characterized will be given below. The average number of secondaries is about three times larger for the uncovered particle ($\delta = 3.48$) as compared to the one covered with C_{60} ($\delta = 1.15$). The secondary electron emission yield as a function of energy is a smooth function characterized by a broad maximum at a value $\delta_{max}(E_{p\,max})$ [22]. The energy chosen for comparison in Fig. 3 is about the value found for the maximum yields, $E_{p\,max}$, for SiO_2 and carbon. The yields found in these measurements agree with the corresponding δ_{max} for SiO_2 (2.1–4) and carbon in graphitic form (1.0) [22]. These results show that the interaction of electrons with the surface of a single nanoparticle can be used for its chemical characterization. The very small number of charging events necessary to derive δ demonstrates the very high sensitivity of the method. As a chemically even more specific tool the emission of photoelectrons from a nanoparticle is studied using synchrotron radiation [23].

The sensitivity of bulk measurements of secondary-electron emission is also sufficient to detect the number of secondaries for one primary electron [24]. However, it is impossible to determine the probability of a primary electron sticking to the surface with no secondary electron escaping, $P(n = 0)$. Interestingly, this probability can be determined in the nanoparticle experiment and as $P(n = 0, C_{60})$ is 4–5 times larger than $P(n = 0, SiO_2)$ this figure appears to be a comparable material constant as the maximum yield itself.

The interaction of electrons leads to a positive or negative charging of the particle. Interaction of molecules leads to a decrease or an increase in mass when molecules leave the surface or stick to it. In the following, high-resolution NPMS is used for quantitative kinetic studies of these processes.

3.2 *Interaction of molecules with the particle*

After injection and mass analysis the particle shown in Fig. 2 has been subject to a cyclic thermal treatment with the help of the CO_2 laser in order to clean and characterize the prefabricated particle. Figure 4 shows two out of 10 cycles over a period of 10 h each. Laser heating at an intensity of $1.4\ W/cm^2$ ($T = 360$ K) is present during the first hour of such a cycle and then followed by nine hours without IR-laser interaction but continuous mass determination using the visible laser. The temporal mass evolution shown is characterized by three phases. At the beginning of the heating procedure, period A, the particle loses more than 0.25 fg during one 10-s measurement. In the following hour, at constant heating, it loses mass at a rate of about 0.01 fg/h. After the heating is switched off the particle is gaining mass to finally reach nearly its initial mass before the next heating cycle is started.

The mass loss is attributed to the evaporation of molecules from the surface due to the thermal heating of the particle. The

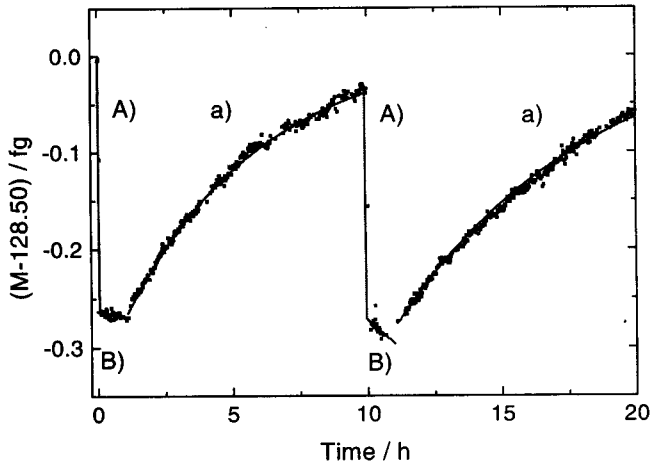

FIGURE 4 Cyclic thermal treatment of the particle, whose mass has been determined earlier, see Fig. 2. During periods A and B, together one hour, the particle is subject to IR-laser heating at an intensity of 1.4 W/cm^2. At $t = 0$ and 10 h the particle looses immediately about 0.25 fg of its original mass. During period B the mass is decreasing at a much slower rate. After turning off the IR heating the mass is slowly increasing during period a. The loss and gain of mass are attributed to the desorption and adsorption of molecules from the residual gas atmosphere in the UHV chamber, which is kept at 2.6×10^{-8} mbar total pressure during this experiment. *Solid lines* represent simulations of the adsorption and desorption according to the kinetics shown schematically in Fig. 5

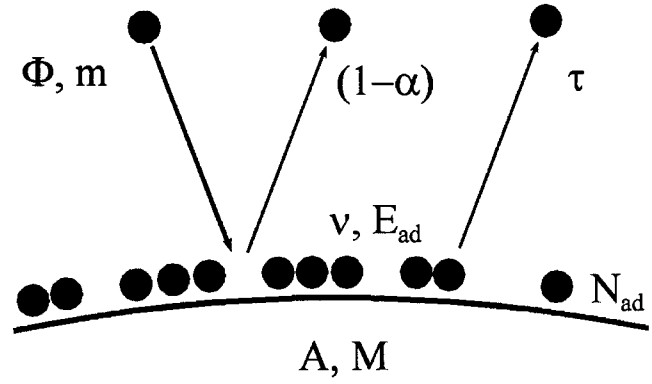

FIGURE 5 Kinetics of the adsorption and desorption processes of molecules, m, to the surface A of a particle, M. Φ is the flux of molecules from the gas phase to the surface. Sticking upon collision occurs with a probability α. N_{ad} is the number of bound molecules. The bond of the molecules to the surface is characterized by the binding energy E_{ad} and its vibrational frequency ν. The average residence time, τ, is a function of these two quantities and the temperature, T, of the particle

gain of mass is related to the adsorption of molecules. Figure 5 depicts the model of the kinetics of adsorption and desorption of molecules to and from the surface. In this model molecules of mass m hit the surface of an area A at a rate $R = \Phi A$. Here Φ is the flux of molecules $\Phi = nv$, where n is the number density of the gas and v its mean velocity. Sticking occurs with a probability, α, where $R_{ad} = \Phi A \alpha$. In general α is a complex quantity depending on several parameters such as the binding energy of the molecule under consideration, the temperature (of the gas and the particle) or the actual coverage, Θ, of the surface.

The rate of desorption, $R_{des} = N_{ad}/\tau$, can be expressed as a function of the mean residence time, τ, of a molecule at the surface and the number of adsorbed molecules, N_{ad}, which occupy the surface sites. τ is a function of the binding energy of the molecule, E_{ad}, and the frequency, ν, at which the molecule tries to escape from the surface. Desorption is described by an Arrhenius type of behavior,

$$\tau = \nu^{-1} \exp(E_{ad}/kT) . \tag{7}$$

In this simple description adsorption and desorption are related to the fundamental physical–chemical quantities, α and E_{ad}.

Adsorption and desorption are detected in the current experiment directly as a mass change, dM/dt. According to the model described in Fig. 5 dM/dt is given by

$$dM/dt = m(R_{ad} - R_{des}) . \tag{8}$$

Depending on the magnitude of the difference of rates, dM/dt is either positive or negative, leading to a net adsorption or desorption process as seen in Fig. 4. In fact desorption is much faster during period A and levels down during B. This indicates that molecules with different binding energies are leaving the particle. This could be due either to different types of molecules or to the same molecules leaving different sites with different binding energies. A closer inspection of Fig. 4 shows that the net rate during period B is almost zero such that R_{des} and R_{ad} (see period a) almost cancel each other. Therefore the binding energy according to (7) can be determined from the time constant of the adsorption (see below).

According to the kinetics model the rate of desorption is strongly dependent on temperature. Therefore, during period a, where T is room temperature the net rate is governed by $R_{ad} \gg R_{des}$. Thus the mass of the particle is increasing at a rate mR_{ad}. For constant α and R_{ad}, M would therefore rise without limit according to the solution of (8). However, as seen in Fig. 4 M is increasing with a saturation behavior. This is typical for a situation where the sticking probability, α, is coverage dependent and the number of places which can be occupied is decreasing as the coverage, $\Theta = (M - M_0)/\Delta M$, increases:

$$dM/dt = mR_{ad}(1 - \Theta) = mR_{ad}\left(1 - \frac{M - M_0}{\Delta M}\right) . \tag{9}$$

The solid line in Fig. 4 is the solution of (9) and describes the behavior

$$M(t) = M_0 + \Delta M\left[1 - e^{-(t-t_0)/T}\right] , \tag{10}$$

with the time constant $T = 1/\Delta M(\mathrm{Rad}\, m) = 5.3$ h during the first 10 h measurement. ΔM, the mass of one monolayer, is 0.23 fg. $\Delta M/m$ is the maximum number of molecules which can be adsorbed in one monolayer. From the apparent exposure rate of 1 ML/5.3 h the partial pressure of the condensing molecules can be estimated to be 7×10^{-11} mbar using the definition of the exposure of one Langmuir (1 ML), 10^{-6} Torr s. Recalling that desorption and adsorption cancel each other during period B the same time constant ($T = 5.3$ h) can be used to evaluate the binding energy of these molecules using (7) and $T = 360$ K (period B). The result is $E_{ad} = 1.2$ eV assuming a typical value for ν of 1×10^{12} s^{-1}.

The origin of the condensing molecules is very likely the particles themselves. 0.5 g of particles in the particle

source give rise to a net surface area of 1 m^2. Using these numbers the corresponding vapor pressure of the molecules adsorbing on the nanoparticle can be estimated to be only 10^{-13} mbar. Fourier-transform infrared (FTIR) absorption measurements of a bulk sample of the native particles show a strong absorption around 3400 cm^{-1} indicating the presence of hydrocarbon-containing molecules.

For cleaning the nanoparticle's surface the laser intensity has been raised. However, above a threshold of 6–7 W/cm^2 heating leads to discharging with a probable loss of the particle. In order to overcome these limitations the particle source chamber and the trapping chamber will be separated in future experiments and particle bake out will be operational in the heated reservoir. For the performance of controlled experiments on the adsorption and desorption of molecules with the present setup the particles were subject to ex situ bake out for about an hour above 600 K prior filling the reservoir.

C_{60} from the effusive beam source has been deposited on a particle in order to further demonstrate the online monitoring capabilities of NPMS. This procedure is shown in Fig. 6 over a period of two days. The stored particle has an initial mass of 124.5 fg which has been determined by a charging experiment prior to the measurement shown in Fig. 6. A C_{60} multilayer has been deposited on the particle in three steps each followed by a period of more than 10 h during which possible desorption of the adsorbed C_{60} at room temperature has been monitored. Deposition rates (periods a–c) were on the order of ~ fg/h, corresponding to monolayers/h. One monolayer has a nominal mass of 1.1 fg assuming a microscopically flat surface of the 500-nm-diameter sphere. The three adsorption steps correspond to about a monolayer each, leading to a net coverage of 4 fg. Within the error limits of the experiment no desorption could be detected during the monitoring periods A–C. An upper limit for the desorption rate of $(5.9 \pm 0.8) \times 10^{-3}$ fg/h, taken from the slight decrease of mass during period A, corresponds to 1.4 C_{60}/s leaving the surface or a rate of 1.5×10^{-6} ML/s. From this rate a lower boundary of the binding energy of 1.1 eV has been estimated using (7) and a pre-exponential factor of $\nu = 4.3 \times 10^{12}$ s^{-1} taken from [7]. In fact the binding energy found in previous work is much larger and therefore no mass decrease is expected in this measurement. In addition, no adsorption of contaminant molecules is detected on the particle following the C_{60} coverage. An additional C_{60} coverage of about 0.3 fg has been added to the particle before further treatment.

In order to actively desorb C_{60}, laser heating at 6.9 W/cm^2 and a corresponding temperature of 500 K has been switched on days after the initial adsorption measurement. NPMS during this measurement is shown in Fig. 7. The particle has a mass of 128.8 fg at the beginning and the laser is on between $t = 0$ and 22.7 min. C_{60} is desorbing during the first 5 min at a rate of (23.4 ± 2.4) fg/h, corresponding to about 5500 C_{60}/s. More than 2.5 fg are removed from the surface in this early period A. During period B the desorption rate drops to $(\sim 1.05 \pm 0.04)$ fg/h (~ 250 C_{60}/s). The change comes about at a coverage of roughly 2 ML of C_{60}. At this coverage the binding energy of C_{60} to the surface increases substantially. Such a change is characteristic for a change from a multilayer desorption to a submonolayer desorption. Considering the uncertainties of the surface roughness and the absolute mass determination we assume that the change in the desorption rates indeed happens at a coverage of 1 ML. From the rates and the particle temperature we determine the binding energy of the multilayer C_{60} to be 1.47 eV and the submonolayer C_{60} to the surface to be 1.53 eV. Possible errors stem from the uncertainty in the temperature determination. The relative change in binding energies is much smaller.

For multilayer C_{60} desorption our value for the binding energy can be compared to that of Hamza and Balooch [7], i.e. (1.41 ± 0.02) eV. Our value is somewhat larger but does not agree so well with the value for the desorption of C_{60} powder, (1.70 ± 0.04) eV, also given by Hamza and Balooch [7]. The authors attribute the difference in activation energies to

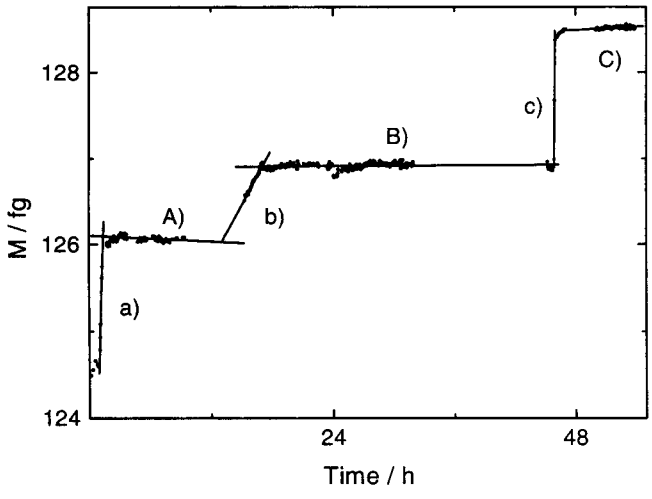

FIGURE 6 C_{60} adsorption to a particle with an initial mass of 124.5 fg. Molecules from an effusive source, not shown in Fig. 1, are adsorbed to the particle during several periods a–c. A total mass increase of more than 4 fg is recorded in this mass spectrum. The adsorption procedure is interrupted during periods A–C in order to check whether C_{60} is desorbing from the room-temperature particle

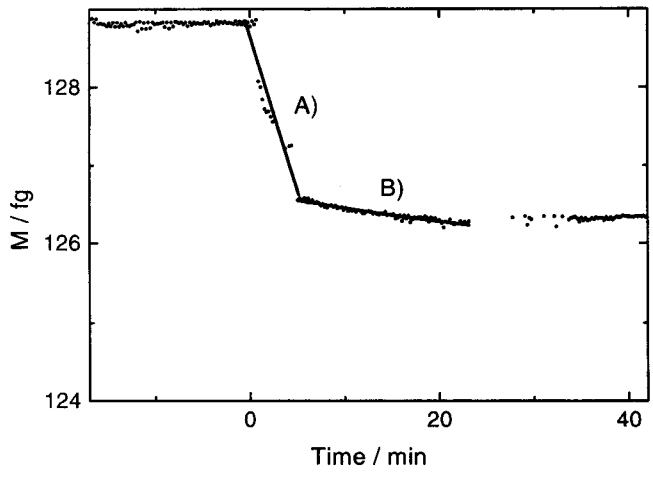

FIGURE 7 Desorption by laser heating ($T = 500$ K) of the C_{60} layer deposited on the particle during the mass determination shown in Fig. 6. During period A more than 2 fg are evaporated at a rate of 23.4 fg/h, see *solid line*. During period B C_{60} molecules are leaving the particle at a much slower rate, 1.1 fg/h, indicating a tighter binding of the last 2 fg to the particle

different structures of multilayer films and powders. Other authors find even larger values for the binding energy of C_{60} to C_{60} of 1.84 eV [8]. Since we do not know the surface structure of our bare particle nor the structure of our multilayer film, our value seems to indicate that the structure of our film is closer to that of a single-crystalline surface than that of a powder. As seen from the sharp drop in the desorption rates, C_{60} is bound to the particle more strongly than C_{60} to a clean SiO_2 surface as found by Moalem et al. [8], i.e. (1.0 ± 0.02) eV. It is gratifying to see that NPMS in combination with IR-laser desorption can be used to determine reliable binding energies. However, a better temperature calibration is necessary to determine more accurate binding energies. At this point it is an open question to what extent a thin C_{60} coverage changes the absorption and emission behavior which connects the heating laser intensity to the particle's temperature. One possible method of calibration is the detection of the blackbody emission curve. Comparison to the integrand of (4) will verify the deviation of Planck's law for small particles and also allow the determination of the index of refraction as a function of temperature. Inspection of the spectral features might allow the distinction of emission from the particle and the coverage. The material system SiO_2 and C_{60} can already be an interesting combination because Si–O vibrations and C–C vibrations are very well separated in wavelength.

4 Conclusions

The present high-resolution NPMS measurements are a first demonstration of a surface-science experiment on a single, isolated and well-localized nanometer-sized particle ($A < 10^{-8}$ cm^2). Temperature-controlled desorption is achieved via IR-laser heating and binding energies have been determined with a precision comparable to TPD experiments on large surfaces.

Due to the long-time online monitoring of NPMS very small adsorption or desorption rates are detectable. In Fig. 5 desorption rates beyond one molecule per second corresponding to $\sim 10^{-3}$ ML/s have been recorded. At improved vacuum conditions this capability can be used to investigate very slow processes at the surface of a single particle. In terms of surface coverage the current mass resolution is 10^{-3} to 10^{-2} ML. This corresponds to about 10^3 to 10^4 molecules. For particles smaller than 50 nm in diameter, therefore single-molecule mass resolution is feasible.

Adsorption and desorption studies using NPMS in combination with laser heating are one method to characterize, prepare and manipulate the surface of a single nanoparticle. However, conventional surface-science experiments make use of various different experimental techniques to characterize the surface in terms of structural information and chemical composition. The probability of emission of secondary electrons has been measured and is characteristic for the chemical composition of the particle's surface. Introduction of other, more specific surface-science techniques to stored nanoparticles is very difficult due to the small surface under consideration. Therefore unconventional methods with very high sensitivity need to be developed.

In terms of composition and molecular structure of the particle and its adsorbates IR-laser heating is a very interesting and rather specific tool which in connection with NPMS can be developed to compare to FTIR absorption studies. In the present case it was used to excite Si–O stretching vibrations of the particle to heat the substrate of the C_{60}. By use of a tunable IR source particle and adsorbate can be excited selectively and the temporal evolution of the particles mass, $M(t)$, can be used to reconstruct an IR spectrum in order to identify the chemical composition of the sample.

Another very versatile tool for the characterization of the chemical composition and crystalline structure is photoelectron spectroscopy (PES). Electron currents from nanometer-sized particles are too small to record photoelectron spectra. However, since the charge state of the particle can be monitored as a function of the excitation energy, UV- and XUV-absorption spectra can be derived with 100% detection efficiency. For this purpose electrons leaving the particle have to be fed back during the experiment in order to avoid charge saturation. Due to the high detection sensitivity of UV photons originating from X-ray absorption/fluorescence experiments X-ray absorption spectra can also be obtained. A dedicated experiment combining NPMS and synchrotron radiation is under construction at BESSY.

The investigation of nanometer-sized surfaces is a rather new field and many unconventional techniques have to be developed to interrogate a single isolated particle at a time. NPMS is a first step in this direction.

ACKNOWLEDGEMENTS The work has been funded by the Deutsche Forschungsgemeinschaft Graduiertenkolleg: 'Thin films and non-crystalline materials' and is currently funded by the German ministry for research (BMBF): 'Investigations of trapped nanoparticles with synchrotron radiation'.

REFERENCES

1 C.E. Kolb, D.R. Worsnop, M.S. Zahniser, P. Davidotis, L.F. Keyser, M.-T. Leu, M.J. Molina, D.R. Hanson, A.R. Ravishankara: In *Laboratory Studies of Atmospheric Heterogeneous Chemistry* (Adv. Ser. Phys. Chem.), ed. by J. Barker (World Scientific, Singapore 1995) p. 771
2 A.C. Gutyon: *Textbook of Medical Physiology*, 6th edn. (Saunders, Philadelphia 1981) Chapt. 39, p. 487
3 J. Blum, G. Wurm, S. Kempf, T. Henning: Icarus **124**, 441 (1996)
4 D. Gerlich, J. Illemann, S. Schlemmer: In *Molecular Hydrogen in Space*, ed. by F. Combes, G. Pineau des Forets (Cambridge University Press, Stanford 2000) pp. 63–69
5 C.C. Chen, C.J. Tao: J. Chem. Phys. **112**, 9967 (2000)
6 V. Pironello, C. Liu, J.E. Roser, G. Vidali: Astron. Astrophys. **344**, 681 (1999)
7 A.V. Hamza, M. Balooch: Chem. Phys. Lett. **198**, 603 (1992)
8 M. Moalem, M. Balooch, A.V. Hamza, W.J. Siekhaus, D.R. Olander: J. Chem. Phys. **99**, 4855 (1993)
9 H.J. Fraser, M.P. Collings, M.R.S. McCoustra, D.A. Williams: MNRAS **327**, 1165 (2001)
10 R.F. Wuerker, H. Shelton, R.V. Langmuir: J. Appl. Phys. **30**, 342 (1959)
11 S. Arnold: J. Aerosol Sci. **10**, 49 (1979)
12 M.A. Philip, F. Gelbard, S. Arnold: J. Colloid Interface Sci. **91**, 507 (1983)
13 B. Krämer, O. Hübner, H. Vortisch, L. Wöste, T. Leisner, M. Schwell, E. Rühl, H. Baumgärtel: J. Chem. Phys. **111**, 6521 (1999)
14 E.J. Davis: Aerosol Sci. Technol. **26**, 212 (1997)
15 S. Schlemmer, J. Illemann, S. Wellert, D. Gerlich: J. Appl. Phys. **90**, 5410 (2001)
16 Synrad, Inc., 4600 Campus Place, Mukilteo, WA 98 275, USA, CO_2 laser, type 48-2 (W)
17 C.F. Bohren, D.R. Huffman: *Absorption and Scattering of Light by Small Particles* (Wiley, New York 1983)
18 E.D. Palik: *Handbook of Optical Constants of Solids* (Academic, San Diego 1998)

19 F. Windisch: Diploma thesis, TU Chemnitz (2001) [http://archiv.tu-chemnitz.de/pub/2001/0079]
20 Merck Company, specific mass $\varrho = (2.0 \pm 0.1)\,\mathrm{g/cm^3}$. Using electron micrographs we determined the diameter of the particles to be $498 \pm 36\,\mathrm{nm}$ (2σ)
21 Simion 3D v.6.0, Lockheed Martin Idaho Technologies (1995)
22 D.R. Lide: *CRC Handbook of Physics and Chemistry* (CRC, Boca Raton, FL 1993) Chapt. 12, p. 107
23 E. Rühl, D. Gerlich, S. Schlemmer, W. Widdra, B. Langer, U. Becker: Construction and testing of a new apparatus for the investigation of trapped nanoparticles with synchrotron radiation. Publication in preparation
24 P. Varga, H. Winter: In *Particle-induced Electron Emission II*, ed. by D. Hasselkamp, H. Rothard, K.-O. Groeneveld, J. Kemmler, P. Varga, H. Winter (Springer Tracts Mod. Phys.) (Springer, Berlin 1992)